CHAPTER VII

$Bi_{12}TiO_{20}$ SYNTHESIZED DIRECTLY FROM BISMUTH (III) NITRATE PENTAHYDRATE AND TITANIUM GLYCOLATE AND ITS ACTIVITY

7.1 Abstract

Pure phase of sillenite structure, $Bi_{12}TiO_{20}$, was directly synthesized using stoichiometric bismuth (III) nitrate pentahydrate and titanium glycolate by co-precipitation. The influence of pH on the structure of $Bi_{12}TiO_{20}$ was studied in the pH range of 3-10. The sillenite structure was characterized using XRD and FTIR. The photo-degradation reaction of 4-nitrophenol (4-NP) was used to study photocatalytic activity of $Bi_{12}TiO_{20}$ as a function of the preparation pH. The rate of decomposition was followed by UV-vis and TOC. The beginning concentration of 4-NP, 44 ppm, decreased to less than 1 ppm within 30 min for all prepared catalysts. It was found that the decomposition rate constant of $Bi_{12}TiO_{20}$ is six times higher than those of either TiO_2 or Bi_2O_3 under the same conditions.

7.2 Introduction

Discovery of new photocatalysts to reduce toxic agents, for solar energy conversion and to split water into hydrogen and oxygen by photocatalytic decomposition is one of the grand challenges for scientists. The semiconducting catalyst, TiO_2, for instance, has been used intensively for degradation of toxic organic impurities diluted in water [1-2]. Although, TiO_2 is capable of decomposing a wide variety of organic and inorganic pollutants, the reactivity and selectivity for some applications, such as large scale applications, are not satisfactory due to a fast recombination rate of photogenerated electron-hole pairs on bulk TiO_2. In order to be usable over a wider range than TiO_2, including the visible region, the band gap engineering of the photocatalyst must be done [3], indicating that, the band gap of catalyst must be one of the factors that need to be concerned.

Recently, it was reported that $Bi_{12}TiO_{20}$ could be used as photocatalyst due to its high photocatalyst activity for decoloration of methyl orange [4-5]. $Bi_{12}TiO_{20}$, which is in the class of $Bi_{12}MO_{20}$ (where M= Ge, Si, or Ti) crystallize on the I23 space group and known as sillenite structure exhibits a number of interesting properties, including piezoelectric, electro-optical, elasto-optical and photoconductive properties [6-7]. The $Bi_{12}TiO_{20}$ crystal has complex structure that composes of two structural units which are TiO_4 tetrahedra and BiO_5 polyhedra, and allows the charge trapping sites. Ti-atoms are located at the corners and at the center of the elementary cell surrounded by four oxygen atoms and BiO_5 polyhedra are arranged by each of 24 bismuth atoms surrounded with five oxygen atoms to form an octahedral arrangement together with stereochemically active $6s^2$ lone electron pair of Bi^{+3} [8]. The photocatalysis mechanism of $Bi_{12}TiO_{20}$ is proposed to be the same as semiconducting. The primary step in the photocatalyst process is to generate electrons and holes within the catalyst particles. The electrons and holes produced by UV-irradiation play a significant role in the formation of an active intermediate species, such as, O_2^-, OH•, H• etc., depending on the reaction condition [9]. In this study, $Bi_{12}TiO_{20}$ synthesized from co-precipitation of bismuth (III) nitrate pentahydrate and titaniun glycolate was used as catalyst to demonstrate the photo-degradation reaction of 4-nitrophenol and determine the degradation rate.

7.3 Experimental

7.3.1 Materials

Titanium dioxide (≥98.5% purity, surface area 12 m^2/g) and 4-nitrophenol (A.R. grade) were purchased from Sigma-Aldrich Chemical Co. Inc. (USA) and used as received. Ethylene glycol (A.R. grade) was purchased from Malinckrodt Baker, Inc. (USA) and purified by fractional distillation at 200°C under nitrogen atmosphere before use. Triethylenetetramine (TETA) was purchased from Facai Polytech. Co. Ltd. (Thailand). Bismuth (III) nitrate pentahydrate (98% purity) was purchased from

Fluka. Nitric acid and ammonium hydroxide (A.R. grade) were supplied from Labscan Asia Co. and Carlo Earba, respectively.

7.3.2 Titanium Glycolate Synthesis

A mixture of titanium dioxide (0.025 mol, 2 g), triethylenetetramine (0.007 mol, 3.7 g) used as a catalyst, and 25 mL of ethylene glycol used as a solvent was heated to the boiling point of EG for 24 hr, followed by separating the unreacted TiO_2 from the solution part. The excess EG and TETA were removed by vacuum distillation to obtain the crude white solid product, followed by washing with acetonitrile and drying in a vacuum desiccator before characterization using FTIR and TGA [10].

FTIR: 2927-2855 cm^{-1} (νC-H), 1080 cm^{-1} (νC-O-Ti bond), and 619 cm^{-1} (νTi-O bond). TGA: a single sharp transition at 340°C and 46.95% ceramic yield corresponding to Ti $(OCH_2CH_2O)_2$.

7.3.3 Catalyst Preparation

Bismuth (III) nitrate pentahydrate was dissolved in nitric acid, and the stoichiometric amount of titanium glycolate was added to the solution with vigorously stirring until the mixture turned clear. The pH of the mixture was adjusted in the range of 3 to 10 using ammonium hydroxide and nitric acid. After stirring for 1 hr, the mixture was centrifuged to separate the precipitate out and washed with water until the filtrate became neutral. The white solid obtained was dried at 60°C and calcined at 300°-600°C.

7.3.4 Material Characterization

FTIR spectroscopic analysis was conducted using a Bruker Instrument (EQUINOX55) with a resolution of 4 cm^{-1}. The solid samples were mixed, pelletized with dried KBr and measured in the transmission mode. Thermal properties were

analyzed by thermogravimetric analysis (TGA) using Du Pont Instrument TGA 2950. The crystallographic phase of the product, $Bi_{12}TiO_{20}$, was characterized using a Rigaku X-ray diffractometer at a scanning speed of 5.0 degree/sec using CuKα as source. The working range was 2θ = 15-60. Both diffuse reflectance ultraviolet spectroscopy and UV-Vis were obtained with a Shimazu UV-2550 spectrometer. The reflectance output from the instrument was converted using Kubelka-Munk algorithm. Particle size analyzer was conducted using Malvern Instrument. The calcination was achieved using a Carbolite Furnace (CFS 1200) with the heating rate of 1°C/min.

7.3.5 Photocatalytic Process

Photocatalytic activity test was carried out in the UV box containing magnetic stirrer. Each reaction suspension was prepared by adding the prepared sample into a 100 ml solution mixture of 44 ppm 4-nitrophenol in water. Prior to irradiation, the suspension was magnetically stirred in the dark for 1 hr to establish adsorption equilibrium. Simultaneously, UV tests without catalysts were investigated to exclude direct photolysis. The suspensions of catalysts in 4-NP were then illuminated using a 100 Watt Hg Philip UV lamp without bubbling oxygen into the solution. The distance between the liquid surface and light source was about 4-5 cm. During photocatalytic testing, the samples were continuously stirred using magnetic stirrer. Sampling was done at the same time intervals for all the samples. The samples were filtered using 0.45 μm Nylon filters before analysis for 4-nitrophenol concentration by UV-Vis spectrometer and TOC analyzer.

7.4 Results and Discussion

7.4.1 Charactrization of $Bi_{12}TiO_{20}$

Generally, $Bi_{12}TiO_{20}$ is prepared by solid-state reaction of Bi_2O_3 and TiO_2 at elevated temperature, however, owing to some inherent limitations this process

yields large grain size of product phase [11]. In this work, highly pure phase of $Bi_{12}TiO_{20}$ was successfully prepared. Its X-ray diffraction pattern was indexed based on JCPDS data card number 34-0097 as the cubic lattice where the unit cell is a=10.174 Å, see fig. 7.1. According to the XRD spectra, the co-precipitated precursors were completely converted to the product structure having single phase of sillenite $Bi_{12}TiO_{20}$. The reason could be due to the fact that the chosen titanium glycolate as precursor is much more moisture stable than commercially available Ti $(OR)_4$ or $TiCl_4$ used in general synthesis [10, 12], and thus provides considerably more time for Ti atoms to arrange into the bismuth crystal.

It was found that the crystallization of $Bi_{12}TiO_{20}$ nano-crystals is influenced by the annealing temperature, time and heating rate [11]. Thus, the importance of the sintering temperature was studied. Fig. 7.2 shows the XRD spectra of samples calcined at 300°-600°C. In the preparation of pure sillenite $Bi_{12}TiO_{20}$, a metastable phase appeared during the formation of $Bi_{12}TiO_{20}$ nanocrystal. Gradual transformation into sillenite phase was found with the sintering temperature changing from 400° to 600°C. At low calcinations temperatures, an amorphous phase was obtained, which slowly changed to the metastable phase with increasing temperature upto 400°C and finally to the cubic sellenite phase at 500°C. Single phase $Bi_{12}TiO_{20}$ was obtained at of 600°C.

FTIR spectra of samples sintered at 300°-600°C are shown in fig. 7.3. Only a broad band at 400-800 cm^{-1} is observed, however, at the sintering temperature, starting from 500°C, the broad band splits into 4 peaks at 457, 525, 586 and 663 cm^{-1}, corresponding to the characteristic peaks of sellenite having Bi-O vibration modes, as reported by Carvalho *et al* [13-14]. This result is in good agreement with the XRD results discussed above and with previous studies on the formation of cubic sillenite structure [11, 13-14]. Increasing the temperature upto 600°C, the spectrum showed sharper peaks, indicating a better alignment of the cubic sillenite structure.

It has been demonstrated that the synthesis of $BaTiO_3$, $SrTiO_3$ and $PbTiO_3$ powders by co-precipitation of stoichiometric of precursors were extremely pH-dependent [15]. Therefore, the effect of pH-dependence onto the formation of $Bi_{12}TiO_{20}$ was studied. The XRD results of $Bi_{12}TiO_{20}$ prepared at various pHs are

shown in fig. 7.4. In this case, for all pH conditions, the XRD patterns did not show significant difference. However, the optimal pH giving only the single phase of sillenite structure is in the range of 3-6. The others showed very low intensity peaks at 26.9 and 33.2 degrees 2 theta with $d_{spacing}$ of 3.306 and 2.693, being characteristics of segregated Bi_2O_3 phase as based on JCPDS data card number 41-1149, monoclinic structure. These main two peaks correspond to 120 and 200 reflections, respectively. It can be seen that the intensity of peaks of this phase becomes stronger with increasing pH. The reason, as discussed previously, is again the use of the moisture stable precursor resulting in appropriate conditions for the reaction to proceed. Furthermore, it has been reported that $Bi(NO_3)_3$ seemed to precipitate at pH above 5, thus at higher pH it tended to be segregate and generate unreacted Bi_2O_3 [12].

The light absorption property of the prepared $Bi_{12}TiO_{20}$ was examined using diffuse reflectance UV-vis spectroscopy with Kubelka-Munk function, as shown in fig 7.5. This technique provides information about the electronic transition and band gap of semiconductors. Feng *et al.* in 2003 assumed that $Bi_{12}TiO_{20}$ is an indirect gap semiconductor similar to TiO_2 and also found that the absorption band of $Bi_{12}TiO_{20}$ showed a steep edge in the visible region due to an intrinsic band transition, not to surface states [16]. In our case, the absorption onset wavelength of $Bi_{12}TiO_{20}$ is around 500 nm which is shifted by 120-130 nm to visible region, as compared to TiO_2. In addition, it has been reported that the onset of Bi_2O_3 is below 443 nm [17], approximately 60 nm blue shift from $Bi_{12}TiO_{20}$. From our data, the calculated energy bands of TiO_2, Bi_2O_3 and $Bi_{12}TiO_{20}$ are 3.18, 2.70 and 2.44 eV, respectively, which is close to the previous work reported on the band gap of these metal oxides.

The particle size distribution of all prepared $Bi_{12}TiO_{20}$ was investigated using particle size analyzer. The prepared catalysts have particle sizes in the range of 15-24 μm, as summarized in table 7.1, indicating the homogeneity of the prepared catalysts.

7.4.2 Photocatalytic Testing

In this study, 4-nitrophenol (4-NP) was used as a test reactant. The decomposition of 4-NP was detected as a function of concentration change using

both UV-Vis and TOC. Both UV-Vis and TOC analyses showed similar results. In this paper, we only show the UV-Vis results because of the ease of calculation of the apparent rate constant. Fig. 7.6 shows the UV-spectra of 4-NP degaradation as a function of reaction time. The concentration of 4 NP rapidly decreases with exposure time. However, it was seen that a small disappearance of 4-NP occurred even in the dark. The reason could be explained in two different possibilities. The first one is based on the intrinsic sillenite type structure of catalyst, allowing the existence of a number of charges trapping site to adsorb some of 4-NP, as discovered in the case of TS-1 and TiO_2 catalysts [18]. The other possibility could be from the mass transfer effect. In photocatalysis, oxygen is known to generate active intermediate species, $OH^{\bullet}$and $O_2^{\bullet-}$, and in this study, the external oxygen was not bubbled into the reaction solution. Thus, only oxygen on the solution surface was contacted, limiting the reaction rate even catalyst concentration was increased. As stated earlier, photocatalyst activity generates electrons and holes within the catalyst particle, leading to the generation of $OH^{\bullet}$ and $O_2^{\bullet}$ radicals. These radicals react with 4-NP, generating other intermediates and finally oxidizing the products to CO_2 and NO_3^-.

Figure 7.7 shows the dependence of activity on the concentration of the photocatalyst. The catalyst concentration in the range of 2-5 g/l was studied. At low catalyst concentrations, 2 and 3g/l, the rate of decomposition reaction shows a detectable dependence on the catalyst concentration. Increasing catalyst concentration up to 4g/l, resulted in very rapid 4 NP decomposition rate and the difference between 4g/l and 5g/l could not be measured accurately. The concentration of 4-NP was decreased to less than 1 ppm (from starting concentration of 44 ppm) within 30 min. The effect of the catalyst concentration seemed to be negligible when increased higher than 4 g/l. This can be due to reaching photon flux limitation and to the shielding effect in which the catalyst particles emit the light instead of absorbing [19]. The concentration of 4g/l was chosen to use in the further study.

By using the equation of $\ln(C_o/C) = k't$, the apparent rate constant of various catalyst concentrations was obtained and are listed in table 7.2. The rate constants show highly nonlinear dependence on the catalyst concentration and the dramatic

increase seen in going from 3 g/l to 4g/l is hard to explain. Since the photoreaction of 4-NP by UV illumination was found to occur to some extent even in the absence of photocatalyst [18]. To correct for this UV exposure tests without catalysts were run to estimate magnitude of the direct photolysis quantitatively.

Although, XRD patterns did not show significant dependence on the pH of the precursor solution, it was still interesting to study whether these catalysts showed any difference in activity. We also wanted to see the effect of phase separation of Bi_2O_3 on the catalyst activity. Fig. 7.8a, b, show plots of 4-NP decomposition as a function of time and precursor solution pH. In addition, the plots of $\ln(C_o/C)$ versus time for all pHs resulted in straight lines and were examined as pseudo-first-order reactions. The apparent rate constants of various catalyst preparation conditions are summarized in table 7.3. The data given in figure 7.8 and table 7.3 show no clear trend and the small variations seen are probably due to experimental artifacts. The catalyst activities of TiO_2 and Bi_2O_3 were also studied for comparison under the same reaction conditions (graphs are not shown). The apparent rate constants of TiO_2 and Bi_2O_3 are much lower, as compared $Bi_{12}TiO_{20}$. This is not surprising since $Bi_{12}TiO_{20}$ has a lower energy band gap, thus higher tendency to generate electron hole-pairs. Furthermore, the catalytic rate constants of $Bi_{12}TiO_{20}$ in our study are much higher than those studied using TS-1 [18]. The reason could be explained, based on the photocatalyst mechanism of $Bi_{12}TiO_{20}$. The photocatalytic process of semiconductors occurs by direct absorption of a photon and generation of electron-hole pairs. For $Bi_{12}TiO_{20}$, 3d level of Ti^{4+} lies between 6s and 6p levels of Bi^{3+}. From previous calculations, the 2.7 eV energy band of Bi_2O_3 was assumed to be located on the top of Bi^{3+} between the 6s and 6p bands [4, 17], and it was reported that the band gap of $Bi_{12}TiO_{20}$ of 2.44 eV results from the excitation of an electron from 6s orbital of Bi^{3+} to 3d orbital of Ti^{4+}.[4] Because of its lower band gap energy, $Bi_{12}TiO_{20}$ could be used for a wide range of applications due to its absorption in a wide range of wavelengths all the way into the visible region, or its high photoconductivity, electro-optical coefficients and holographic sensitivity in the red spectral region [8]. In addition, we note that the photocatalytic reaction in this study using $Bi_{12}TiO_{20}$ catalyst was carried out at neutral pH while many studies report that the rate of 4-NP

decomposition using commercially available TiO_2 was faster at lower pH and showed the highest activity at pH 3 [20-21].

7.5 Conclusions

$Bi_{12}TiO_{20}$, having the sillenite structure was, successfully synthesized using stoichiometric bismuth (III) nitrate pentahydrate and titanium glycolate by co-precipitation. The best pH for preparation of pure phase sillenite structure is 3-6. $Bi_{12}TiO_{20}$ showed much higher rates of photocatalytic activity for photodegradation reaction of 4-nitrophenol (4-NP) compared to TiO_2 and Bi_2O_3. Photodegradation of 44 ppm of 4-NP was essentially complete in less than 30 minutes.

7.6 Acknowledgements

This research work is supported by the Postgraduate Education and Research Program in Petroleum and Petrochemical Technology (ADB) Fund, Ratchadapisake Sompote Fund, Chulalongkorn University and the Thailand Research Fund (TRF).

7.7 References

[1] S. B. Dhananjay, G. P. Vishwas, A. C. M. B.Anthony, Water Res. (2003) 1223.

[2] S. Yasushi, I. Keita, O. Makoto, A. Masakazu, Appl. Catal. 254 (2003) 251.

[3] A. Masakazu, T. Masoto, J. Catal. 216 (2003) 505.

[4] W. F. Yao, H. Wang, X. H. Xu, X. F. Cheng, J. Huang, S. X. Shang, X. N. Yang , M. Wang, Appl. Catal. A 243 (2003) 185.

[5] W. F. Yao, H. Wang, X. H. Xu, X. F. Cheng, J. Huang, S. X. Shang, X. N. Yang , M. Wang, J. Mol. Catal. A 202 (2003) 305.

[6] I. F. Vasconcelos, M. A. Pimenta, A. S. B. Sombra, J. Mat. Sci. 36 (2001) 587.

[7] I. V. Kityk, A. Majchrowski, J. Ebothe, B. Sahraoui, Opt. Commun. 236 (2004) 123.

[8] V. Marinova, M. L. Hsieh, S. H. Lin, K. Y. Hsu, Opt. Commun. 203 (2002) 377.

[9] M. Masaya, A. Masakazu, J. Photochem. Photobiol. C 3 (2003) 225.

[10] N. Phonthammachai, T. Chairassameewong, E. Gulari, A. M. Jamieson, S. Wongkasemjit, J. Met. Mat. Min. 12 (2003) 23.

[11] W. F. Yao, H. Wang, X. H. Xu, X. F. Cheng, J. Huang, S. X. Shang, X. N. Yang, M. Wang, J. Mater. Sci. Lett. 21 (2002) 1903.

[12] A. M. Umabala, M. Suresh, A. V. Prasadarao, Mater. Lett. 44 (2000) 175.

[13] J. F. Carvalho, R. W. A. Franco, C. J. Magon, L. A. O. Nunes, F. Pellegrini, A. C. Hernandes, Mater. Res. 2 (2) (1999) 87.

[14] J. F. Carvalho, R. W. A. Franco, C. J. Magon, L. A. O. Nunes, F. Pellegrini, A. C. Hernandes, Opt. Mater. 13 (1999) 333.

[15] A. V. Prasadarao, M. Suresh, S. Komarneni, Mater. Lett. 25 (1999) 75.

[16] K. Akihito, I. Mikami, Chem. Lett. 10 (1998) 1027.

[17] K. Guranathan, Int. J. Hydrogen Energy. 29 (2004) 933.

[18] G. D. Lee, S. K. Jung, Y. J. Jeong, J. H. Park, K. T. Lim, B. H. Ahn, S. S. Hong, Appl. Catal. A 239 (2003) 197.

[19] W. F. Yao, H. Wang, X. H. Xu, X. F. Cheng, J. Huang, S. X. Shang, X. N. Yang, M. Wang, J. Mater. Lett. 57 (2003) 1899.

[20] M.E. Zorn, Photocatalytic oxidation of gas-phase compounds in confined areas: investigation of multiple component systems, Proc. of the 13th Annual Wisconsin Space Conferrence, Green Bay, WI, 14-15 August 2003, Wisconsin Space Grant Consortium, 2003.

[21] J. F. Mano, D. Koniarova, R. L. Reis, J. Mater. Sci. 14 (2003) 127.

Table 7.1 The average particle size of prepared $Bi_{12}TiO_{20}$

pH	Average particle size (μm)
3	20.0
4	18.8
5	22.9
6	21.3
7	23.7
8	16.4
9	16.3
10	15.0

Table 7.2 The apparent rate constants as a function of concentration of $Bi_{12}TiO_{20}$ catalyst

Concentration (g/l)	2	3	4	5
Apparent reaction rate constant (min^{-1})	0.018	0.025	0.135	0.142

Table 7.3 The apparent rate constants of $Bi_{12}TiO_{20}$ catalysts as a function of the precursor solution pH, TiO_2 and Bi_2O_3

Catalyst	Apparent reaction rate constant (min^{-1})
$Bi_{12}TiO_{20}$ precipitated at pH3	0.142
$Bi_{12}TiO_{20}$ precipitated at pH4	0.131
$Bi_{12}TiO_{20}$ precipitated at pH5	0.110
$Bi_{12}TiO_{20}$ precipitated at pH6	0.126
$Bi_{12}TiO_{20}$ precipitated at pH7	0.163
$Bi_{12}TiO_{20}$ precipitated at pH8	0.170
$Bi_{12}TiO_{20}$ precipitated at pH9	0.135
$Bi_{12}TiO_{20}$ precipitated at pH10	0.141
TiO_2	0.002
Bi_2O_3	0.042

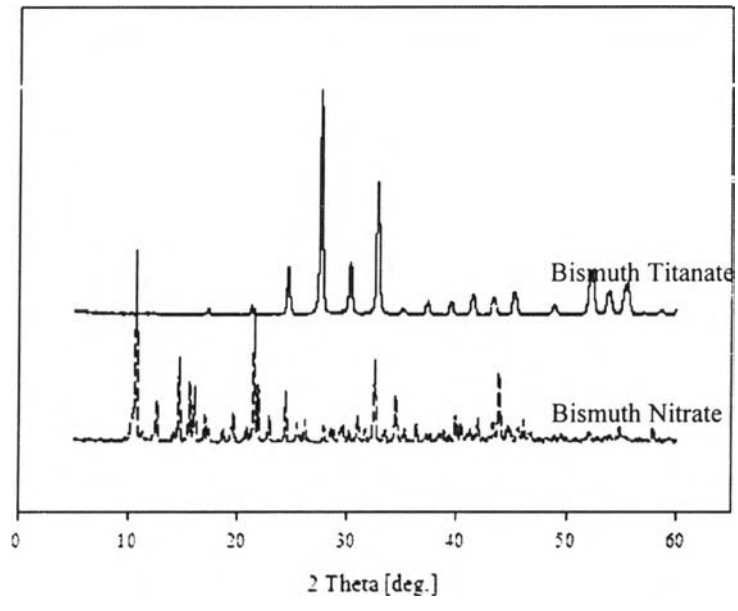

Figure 7.1 XRD patterns of bismuth (III) nitrate pentahydrate precursor and the prepared $Bi_{12}TiO_{20}$ catalyst.

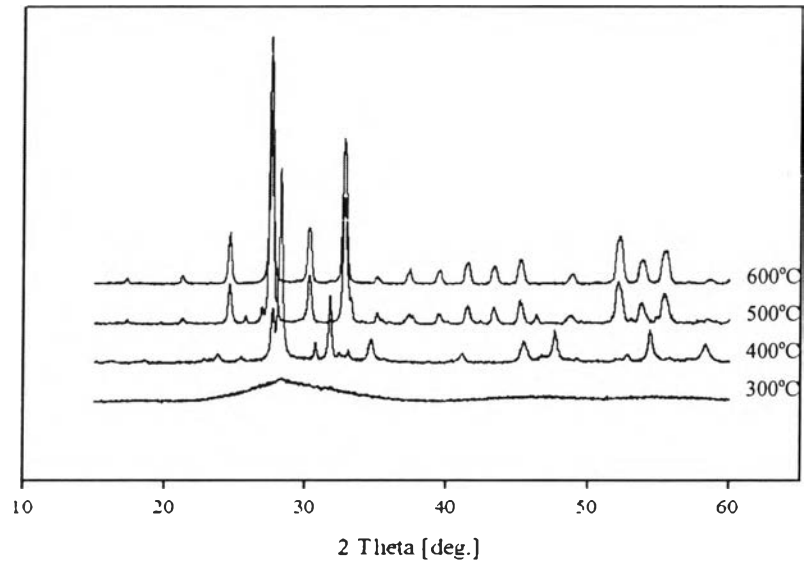

Figure 7.2 XRD spectra of $Bi_{12}TiO_{20}$ sintered at 300°-600°C.

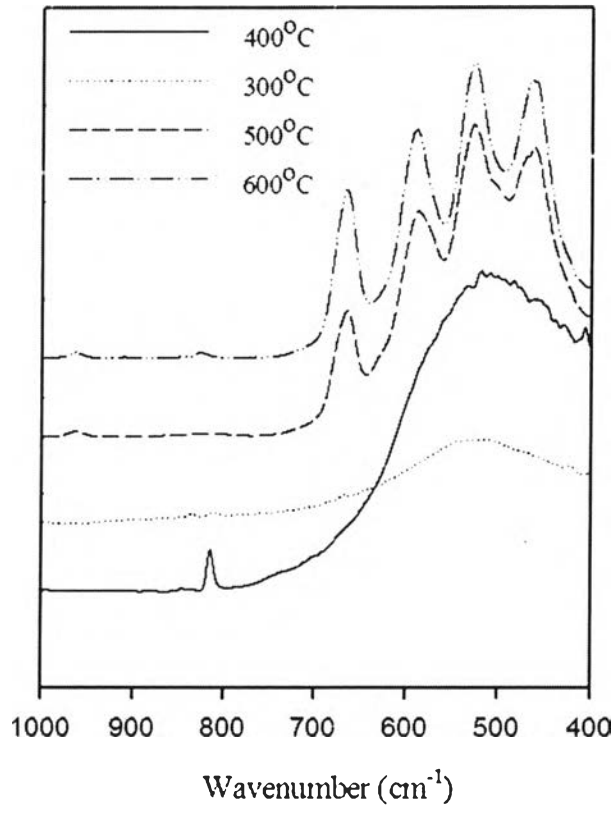

Figure 7.3 FTIR spectra of $Bi_{12}TiO_{20}$ sintered at 300°-600°C.

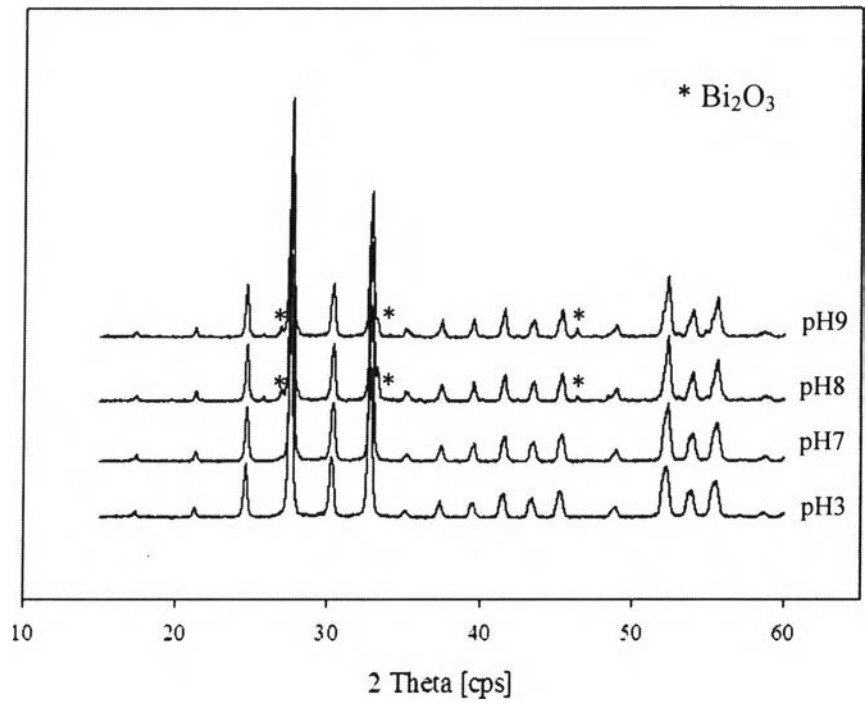

Figure 7.4 XRD patterns of $Bi_{12}TiO_{20}$ prepared at various pHs.

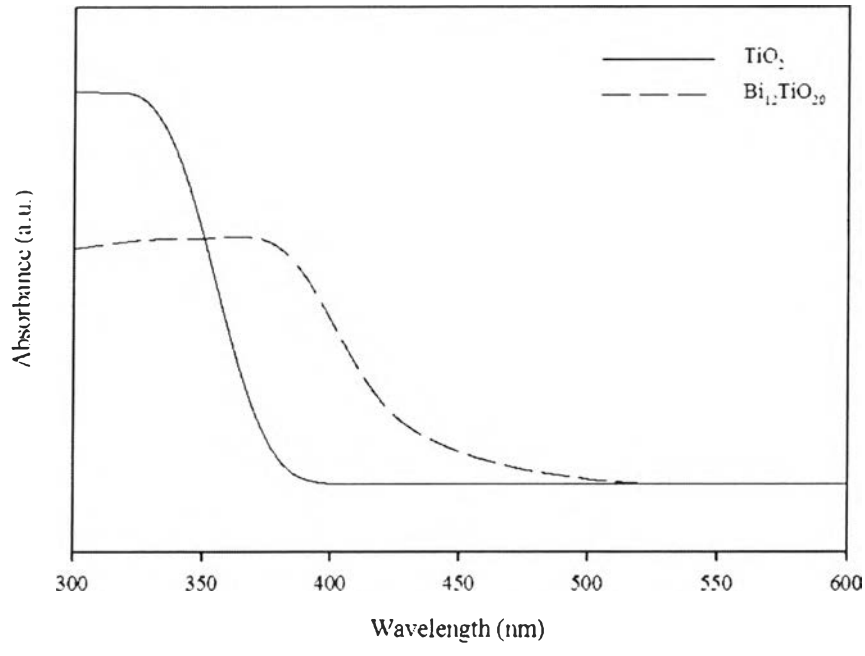

Figure 7.5 DRUV spectra of TiO_2 and $Bi_{12}TiO_{20}$.

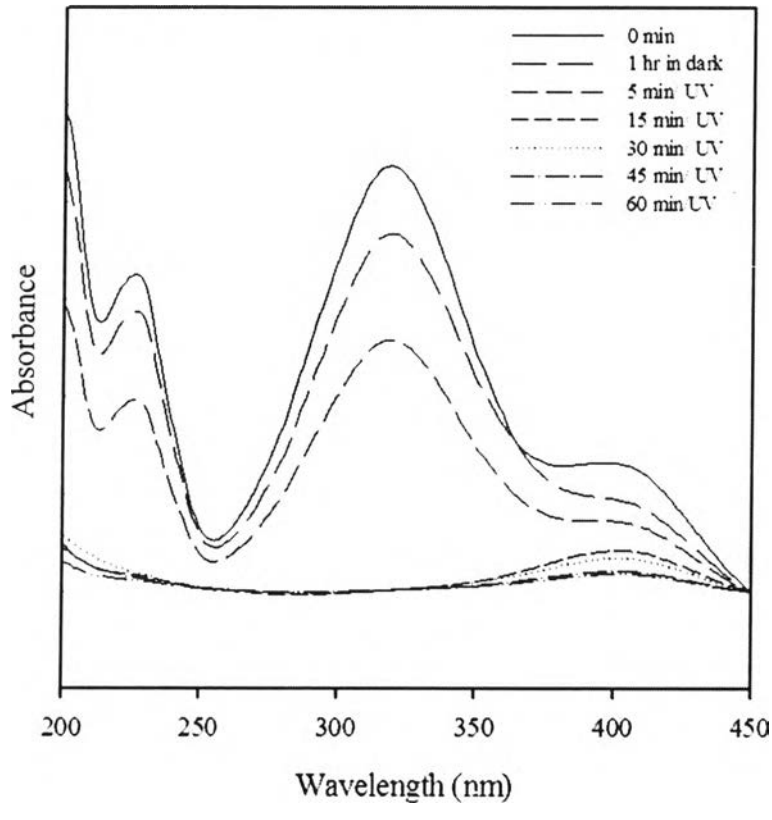

Figure 7.6 UV-vis absorption spectra 4-nitrophenol degraded by $Bi_{12}TiO_{20}$ catalyst and taken at the beginning, after 30 min in dark and after irradiation for 5, 15, 30 and 60 min.

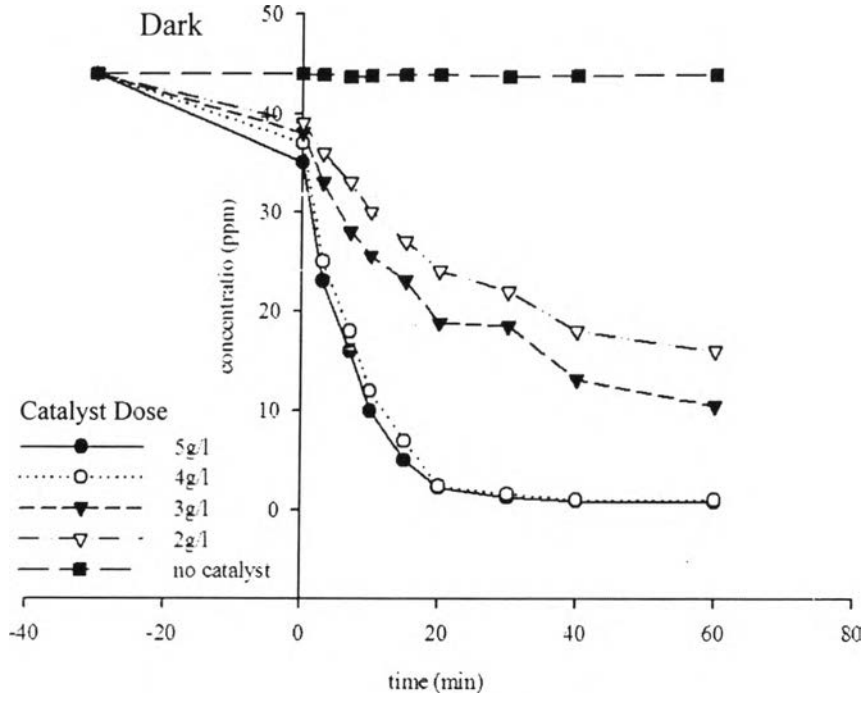

Figure 7.7 Plots of 4-NP concentration change versus times at various catalyst concentrations.

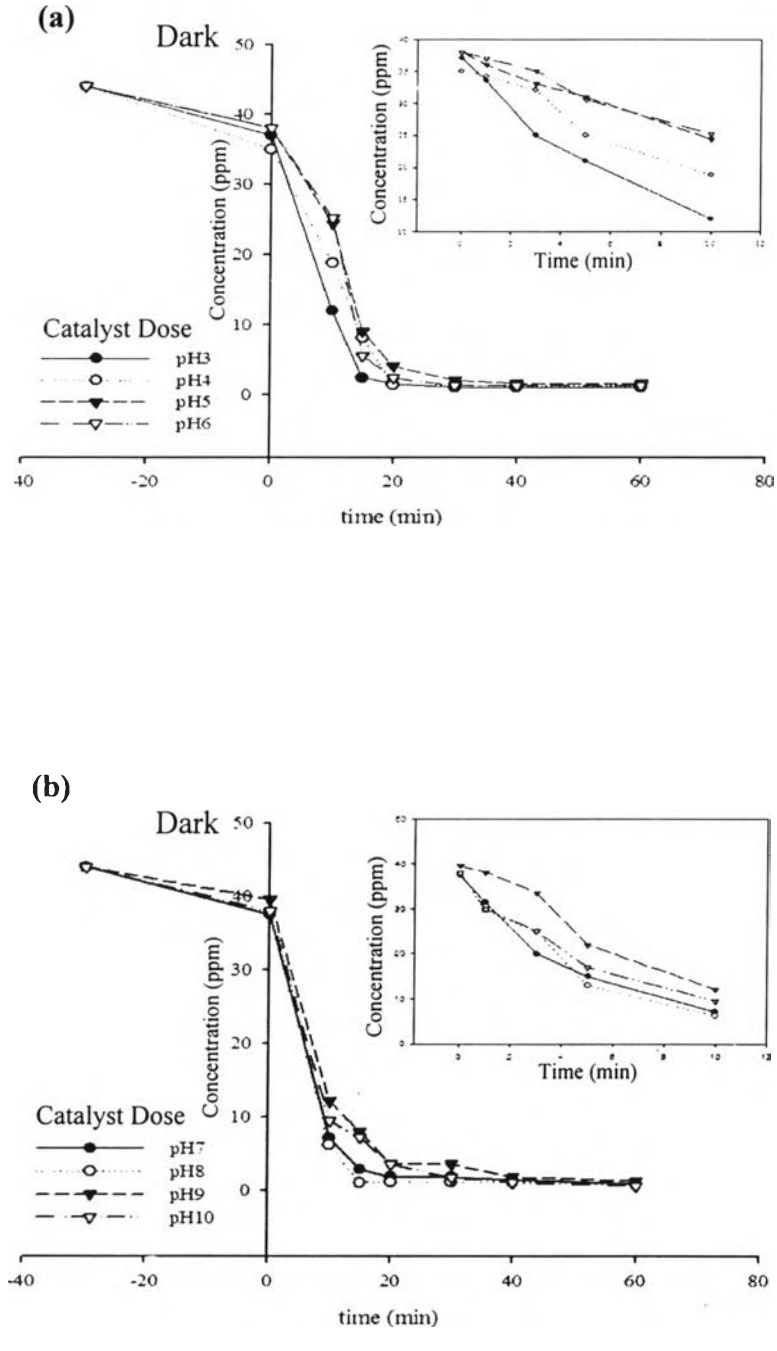

Figure 7.8 Plots of 4-NP concentration change versus times at various pHs.